

DESIGN, FABRICATION, AND TESTING OF
SUPERCONDUCTING RF CAVITIES FOR HIGH AVERAGE
BEAM CURRENTS

By

David Joseph Meidlinger

A DISSERTATION

Submitted to
Michigan State University
in partial fulfillment of the requirements
for the degree of

DOCTOR OF PHILOSOPHY

Department of Physics and Astronomy

2007

UMI Number: 3264196

INFORMATION TO USERS

The quality of this reproduction is dependent upon the quality of the copy submitted. Broken or indistinct print, colored or poor quality illustrations and photographs, print bleed-through, substandard margins, and improper alignment can adversely affect reproduction.

In the unlikely event that the author did not send a complete manuscript and there are missing pages, these will be noted. Also, if unauthorized copyright material had to be removed, a note will indicate the deletion.

UMI[®]

UMI Microform 3264196

Copyright 2007 by ProQuest Information and Learning Company.

All rights reserved. This microform edition is protected against unauthorized copying under Title 17, United States Code.

ProQuest Information and Learning Company
300 North Zeeb Road
P.O. Box 1346
Ann Arbor, MI 48106-1346

ABSTRACT

DESIGN, FABRICATION, AND TESTING OF SUPERCONDUCTING RF CAVITIES FOR HIGH AVERAGE BEAM CURRENTS

By

David Joseph Meidlinger

For high current applications, it is desirable for the cavity shape to have a low longitudinal loss factor and to have a high beam-breakup threshold current. This dissertation describes three different cavities designed for this purpose: a six-cell elliptical cavity for particles traveling at the speed of light, a two-cell elliptical cavity for subluminal particle speeds, and a single cell cavity which uses the TM₀₁₂ mode for acceleration. SUPERFISH simulations predict the peak fields in both of the elliptical cavities will not exceed the TeSLA values by more than 10% but both will have 28.7% larger apertures. The elliptical designs assume the bunch frequency equals the accelerating mode frequency. The beam pipe radius is chosen so that the cutoff frequency is less than twice that of the accelerating mode. Hence all of the monopole and dipole higher-order modes (HOMs) that can be driven by a Fourier component of the beam have low loaded Q values. This simplifies the problem of HOM damping. The TM₀₁₂ cavity is predicted to have much higher peak fields than a π -mode elliptical cavity, but offers potential advantages from its simplified shape; it is essentially a circular waveguide with curved end plates. This basic shape results in easier fabrication and simplified tuning. Two prototype two-cell cavities were fabricated and tested at cryogenic temperatures without beam.

ACKNOWLEDGMENTS

I would like to thank my adviser, Walter Hartung, for his guidance, his professionalism, and his many helpful conversations throughout the years. I am the most grateful for the unequivocal support, heartfelt encouragement, and selfless sacrifice of my wife; Without her, none of this would be possible. This work was supported by the National Science Foundation and the National Superconducting Cyclotron Laboratory Fellowship.

Contents

| | | |
|----------|----------------------------------------------------------------------|-----------|
| 1 | Introduction | 1 |
| 1.1 | Linear Accelerators | 4 |
| 1.1.1 | Energy Recovery Linacs | 6 |
| 1.2 | Radio-Frequency Cavities | 7 |
| 1.2.1 | The Elliptical Cavity | 8 |
| 1.2.2 | Superconductivity | 12 |
| 1.2.3 | Issues Driving Cavity Design | 14 |
| 1.2.4 | Outline | 16 |
| 2 | Superconducting Cavity Design | 18 |
| 2.1 | Waveguide Modes | 18 |
| 2.2 | General Expansion of Electromagnetic Fields Inside a Hollow Cavity . | 23 |
| 2.3 | Applications | 25 |
| 2.3.1 | Lossless Cavity | 25 |
| 2.3.2 | Cavity with Losses and Quality Factor | 25 |
| 2.3.3 | Wall Losses | 28 |
| 2.3.4 | External Ports and External Q | 30 |
| 2.3.5 | Slater's Theorem | 36 |
| 2.4 | Cavity Figures of Merit | 37 |
| 2.4.1 | Accelerating Gradient and Transit Time Factor | 37 |
| 2.4.2 | Quality Factor and Geometry Factor | 39 |
| 2.4.3 | Geometric Shunt Impedance | 40 |
| 2.4.4 | Surface Electric Field Ratio | 41 |
| 2.4.5 | Surface Magnetic Field Ratio | 41 |
| 2.4.6 | Cell-to-cell Coupling | 42 |
| 2.4.7 | Longitudinal Loss Factor | 43 |
| 3 | Six-Cell Elliptical Cavity | 47 |
| 3.1 | The Approach to High Beam Currents | 49 |
| 3.2 | Six-Cell Design | 52 |
| 3.3 | Higher Order Modes of Interest | 58 |
| 4 | Two-Cell Elliptical Cavity | 65 |
| 4.1 | Two-Cell Cavity Design | 65 |
| 4.1.1 | SUPERFISH Simulations | 65 |
| 4.2 | Higher Order Modes of Interest | 69 |

| | |
|----------------------------------------------------------------------|------------|
| 5 Prototyping | 73 |
| 5.1 Fabrication | 73 |
| 5.1.1 Electron Beam Welding | 74 |
| 5.1.2 Waveguide Coupling Measurements and Choice of Beam Tube Length | 77 |
| 5.1.3 Bead Pulls | 84 |
| 5.2 Testing | 86 |
| 5.2.1 Antenna Measurements | 87 |
| 5.2.2 Cavity Preparation | 90 |
| 5.2.3 Vertical Tests | 96 |
| 6 Single-Cell HOM Cavity | 112 |
| 6.1 Concept | 112 |
| 6.1.1 Pillbox Trends | 114 |
| 6.2 Cavity Design | 124 |
| 6.2.1 Rounding the Corners | 126 |
| 6.2.2 Adding the Beam Tubes | 128 |
| 6.2.3 Loss Factor | 132 |
| 6.2.4 Comparison with SOLEIL Cavity | 134 |
| 7 Conclusion | 136 |
| 7.1 Summary | 136 |
| 7.2 Implications | 137 |
| 7.3 Possible Future Work | 138 |
| A Waveguide Modes | 140 |
| A.1 Maxwell's Equations | 140 |
| A.2 Circular Waveguide Modes | 145 |
| A.2.1 Transverse Electric Modes | 145 |
| A.2.2 TE ₁₁ Mode | 149 |
| A.2.3 Transverse Magnetic Modes | 151 |
| A.2.4 TM ₀₁ Mode | 152 |
| B General Expansion of Electromagnetic Fields in a Cavity | 154 |
| B.1 The Complete Orthogonal Set | 154 |
| B.1.1 The Solenoidal Fields | 155 |
| B.1.2 The Irrotational Fields | 159 |
| B.2 Time Evolution of the Expansion Coefficients | 162 |
| C Analysis of CW RF Measurements | 167 |
| C.1 Direct Method | 168 |
| C.2 Indirect Method Using $\frac{P_i}{P_f}$ | 169 |
| C.3 Graphical Assessment of Systematic Errors | 172 |
| <i>Bibliography</i> | 174 |

List of Figures

| | | |
|------|------------------------------------------------------------------------------------------------|----|
| 1.1 | TM01 field pattern | 8 |
| 1.2 | Geometrical parameters used in designing the elliptical cell shape . . | 9 |
| 1.3 | The dispersion diagram for the TM010 passband. | 10 |
| 1.4 | Multicell elliptical cavity cartoon | 11 |
| 1.5 | The cell-to-cell variation in field intensity for a passband | 11 |
| | | |
| 3.1 | ERL block diagram | 49 |
| 3.2 | Cartoon of HOM and Low-frequency bunch spectrum | 51 |
| 3.3 | Cartoon of HOM and High-frequency bunch spectrum | 52 |
| 3.4 | Screenshot of the automated interface to SUPERFISH | 60 |
| 3.5 | 6-cell cavity shape and electric field lines of the π -mode | 61 |
| 3.6 | The surface electric and magnetic fields for the 6-cell cavity | 61 |
| 3.7 | Field flatness plot for the 6-cell cavity | 62 |
| 3.8 | Six-cell monopole HOM coupling strength | 62 |
| 3.9 | The R/Q s for the monopole modes as a function of frequency. | 63 |
| 3.10 | Six-cell dipole HOM coupling strength | 63 |
| 3.11 | The R/Q s for the dipole modes as a function of frequency. | 64 |
| | | |
| 4.1 | 2-cell cavity shape and electric field lines | 66 |
| 4.2 | 2-cell cavity surface electric and magnetic fields | 67 |
| 4.3 | 2-cell cavity E_z along axis | 68 |
| 4.4 | 2-cell and 6-cell cavity transit time factors | 69 |
| 4.5 | Two-cell monopole HOM coupling strength | 71 |
| 4.6 | The R/Q s for the monopole modes are plotted vs. frequency. | 71 |
| 4.7 | Two-cell dipole HOM coupling strength | 72 |
| 4.8 | The R/Q s for the dipole modes of the two-cell cavity as a function of frequency. | 72 |
| | | |
| 5.1 | Picture of 2-cell cavity half-cells | 74 |
| 5.2 | Picture of electron beam welding | 76 |
| 5.3 | Picture of a completed 2-cell niobium cavity | 77 |
| 5.4 | Conceptual drawing of the 2-cell cavity | 79 |
| 5.5 | Cartoon of waveguide coupling field pattern | 80 |
| 5.6 | Drawing of waveguide coupler test setup | 81 |
| 5.7 | Measured waveguide coupling Q_{ext} | 82 |
| 5.8 | Dependence of waveguide Q_{ext} on the gap distance | 83 |
| 5.9 | 2-cell cavity beadpull | 84 |

Images in this dissertation are presented in color.

| | | |
|------|-----------------------------------------------------------------------------|-----|
| 5.10 | Diagram of the vertical test setup in the Dewar | 87 |
| 5.11 | Measured Q_{ext} for vertical test input coupler | 89 |
| 5.12 | Measured Q_{ext} for vertical test pickup probe | 90 |
| 5.13 | Picture of BCP in the acid room | 91 |
| 5.14 | 2-cell cavity ready for BCP | 92 |
| 5.15 | High pressure rinse of the 2-cell cavity | 93 |
| 5.16 | The 2-cell cavity attached to the insert while in the clean room | 95 |
| 5.17 | RF system block diagram | 98 |
| 5.18 | First round of Q_0 measurements for the first 2-cell cavity | 103 |
| 5.19 | Second round of Q_0 measurements for the first 2-cell cavity | 104 |
| 5.20 | Zero-mode and π -mode peak magnetic fields | 105 |
| 5.21 | Q_0 measurements of the second 2-cell cavity | 106 |
| 5.22 | Residual resistance estimate | 107 |
| 5.23 | Change in π -mode frequency with pressure | 109 |
| 5.24 | Lorentz force detuning of the 2-cell cavity | 110 |
| 5.25 | Second 2-cell cavity peak magnetic fields | 111 |
| | | |
| 6.1 | A cartoon of the HOM cavity electric field pattern | 113 |
| 6.2 | Pillbox TM012 transit time vs. particle speed | 117 |
| 6.3 | Pillbox TM01 transit time vs. length/radius | 118 |
| 6.4 | Pillbox trend for the maximum $\frac{R}{Q}$ | 120 |
| 6.5 | Pillbox TM01 p G increases with p | 121 |
| 6.6 | Pillbox trend for $\frac{B_p}{E_{\text{acc}}}$ | 122 |
| 6.7 | Pillbox trend for the number of parasitic modes. | 123 |
| 6.8 | A comparison of TM010 and TM01 p magnetic field patterns | 125 |
| 6.9 | $\frac{B_p}{E_{\text{acc}}}$ as a function of radius of curvature | 127 |
| 6.10 | $\left(\frac{R}{Q}\right) G$ as a function of radius of curvature | 128 |
| 6.11 | $\frac{B_p}{E_{\text{acc}}}$ as a function of radius of curvature | 129 |
| 6.12 | $\left(\frac{R}{Q}\right) G$ as a function of radius of curvature | 130 |
| 6.13 | TM012 cavity electric field lines from SUPERFISH | 131 |
| 6.14 | TM012 cavity axial electric field profile | 133 |
| 6.15 | TM012 cavity surface electric and magnetic fields | 133 |
| 6.16 | Snapshots of the short range wake in the TM012 cavity | 134 |
| 6.17 | Scale drawing of the TM012 cavity and a SOLEIL cavity | 135 |
| | | |
| C.1 | The “Duality Triangle” | 173 |

List of Tables

| | | |
|-----|-------------------------------------------------------------------------------------------------------------------------|-----|
| 3.1 | 6-cell midcell parameter list and figures of merit | 56 |
| 3.2 | 6-cell endcell parameter list and cavity figures of merit | 57 |
| 4.1 | 2-cell parameter list and figures of merit | 66 |
| 4.2 | 2-cell figures of merit comparison | 70 |
| 5.1 | Measured Q_0 drop in 2-cell cavity tests | 111 |
| 6.1 | Best TM012 values of $\frac{B_p}{E_{acc}}$ and $\frac{R}{Q}$ for a pillbox | 126 |
| 6.2 | $\frac{B_p}{E_{acc}}$ and $\frac{R}{Q}$ for a pillbox $\left(\frac{a}{l} = 0.425\right)$ with rounded corners | 127 |
| 6.3 | $\frac{B_p}{E_{acc}}$ and $\frac{R}{Q}$ for a pillbox $\left(\frac{a}{l} = 0.350\right)$ with rounded corners | 129 |
| 6.4 | Geometrical parameters of the TM012 cavity | 131 |
| 6.5 | Figures of merit and field levels for the TM012 cavity as compared to SOLEIL | 135 |

Chapter 1

Introduction

Since the late nineteenth century, advances in electrical and vacuum technology have enabled scientists to probe the properties of matter by giving a beam of charged particles a large kinetic energy and then allowing that beam to collide with a target material: Advances in electrical technology enabled high voltages to be produced, which allowed particles to have high energy; Advances in vacuum technology removed most of the air so that the beam only collided with the intended target. As an example, consider an early method for producing a high voltage by creating a large direct current with a parallel bank of voltaic cells and passing the current through a large inductor. By opening the circuit, the magnetic field collapsed and, by Faraday's law, the energy stored in the magnetic field produced an electric field. Under the right conditions, the electric field was large enough for electrons to overcome the attractive forces of ions in the lattice of the metal electrode and leave the surface (a process generally known as field emission), producing a spark. By encasing the electrodes in an evacuated chamber containing a low-pressure gas, the electron beam collided with the gas atoms and produced the characteristic line spectra of the gas atoms. Further advances made even higher voltages possible, and x-rays were discovered experimentally when an electron beam with thousands of electron volts of energy collided with a solid metal electrode. These x-rays were quickly used to show by diffraction exper-

iments that the metal electrode did indeed consist of a lattice of individual atoms. In the early twentieth century, electrostatic voltages on the order of a million volts could be produced with a Cockroft-Walton generator which allowed experimenters to study nuclear reactions. The use of alternating electric fields eventually proved to be superior for producing even higher beam energies corresponding to several millions of volts. The advances in accelerator physics during the first half of the twentieth century were primarily focussed on producing beams of higher energies, enabling further study of subatomic particles. However, the size of the beam also increased with beam energy, and the practical limitations on the size of a beam limited the final energy. The development of strong focussing in the 1950's separated the focussing requirements, and therefore the beam size, from the beam energy, allowing even higher energies to be achieved. The Tevatron, a modern high-energy accelerator at Fermilab, produces a final interaction energy equivalent to one trillion volts, a remarkable increase by twelve orders of magnitude in less than a century.

The goal of accelerator physics is generally to deliver a high flux of particle energy to a chosen target. This may be done with high beam energy, high beam current, or by decreasing the beam emittance (*i.e.* by decreasing the amount of phase space occupied by the beam): The particular application determines the significance of these three areas of energy, current, and emittance. For example, a hospital may use a cyclotron to artificially produce radioactive isotopes for cancer therapy. Since relatively small samples are needed, generating large beam currents at high energy is not necessary. In contrast, a facility designed for transmutation of radioactive waste [1] would ideally use the largest feasible beam current to convert waste at the highest possible rate. Facilities which use a primary beam to produce a secondary beam often need the highest possible primary beam current to produce the "brightest" secondary beam. This is the case for numerous x-ray light sources [2-4] which produce x-rays by accelerating electrons and for the Spallation Neutron Source [5] at Oak Ridge National Laboratory which uses a proton beam to produce spalled neutrons. Electron

microscopy serves as an example where there is ample beam energy and current for the application, but the beam optics limits the resolution, and therefore usefulness, of the device.

The development of superconducting cavities for accelerating charged particles has enabled new applications not previously possible with normal-conducting structures. The low dissipative power losses and high quality factor of superconducting cavities permit continuous wave (CW) operation at high field. CW operation means that energy is continuously delivered to the cavities without interruption, in contrast to pulsed operation where the power is periodically switched off and back on. Also because of the low losses, the aperture may be large, reducing interactions between the beam and higher order modes (HOMs) of the cavity. This smaller interaction has the advantage of reducing the heating of the cavity due to beam energy dissipating in the HOMs, while also increasing the threshold current for beam instabilities caused by HOMs. The advancement of superconducting technology has therefore resulted in a proliferation of the number of high beam current accelerator projects. A number of projects rely on superconducting cavities operating in an energy-recovery mode to accelerate a low-emittance electron beam for the purpose of producing x-ray radiation. The energy-recovery linear accelerator (ERL) concept has been demonstrated at Thomas Jefferson National Accelerator Facility [6]. ERL projects such as the Cornell ERL and 4GLS in Daresbury, United Kingdom are underway. Electron storage rings have historically been used for high brightness x-ray sources. Because the electrons continually circulate through the ring, a relatively small number of cavities is needed to replenish the energy lost to collisions and to radiation. The x-rays produced, whether by a linear accelerator or synchrotron, have found numerous uses in fields such as condensed matter physics, material science, biology, and medicine. Scattering experiments can reveal information about the onset of phase transitions, the atomic lattice of new materials, and the molecular structure of proteins and viruses.

Interest in superconducting cavities has increased since the recent decision to use

this technology for the proposed International Linear Collider (ILC), the highest energy linear accelerator conceived to date. This global commitment to superconducting radio frequency (SRF) cavities has spurred research and development efforts for existing accelerators and new projects [7]: the B-factories at KEK and Cornell, the CEBAF upgrade at JLAB, SNS at Oak Ridge, XFEL at DESY, ERL projects at Cornell, 4GLS at Daresbury, ELBE at Forschungszentrum Rossendorf, BESSY-ERL, and the ERL/FEL at JLAB.

Since a large part of this thesis describes the design and prototyping of cavities intended for use with an ERL, the following sections provides general background information on the development of linear accelerators. The distinction of a linear accelerator operating with energy recovery may then be better understood.

1.1 Linear Accelerators

The first linear accelerator (linac) using alternating fields was constructed and tested by Wideröe in 1927 [8, Sec.1.1]. A voltage of 25 kV at 1 MHz was applied to a single drift tube with the entrance and exit tubes grounded. Singly charged ions would arrive at the first accelerating gap at the peak of the radio frequency (RF) cycle, gaining 25 keV of energy. The ions then travelled through a drift tube which shielded them from the electric fields for half a RF period. The ions then emerged from the drift tube where the electric field at the next accelerating gap was at its peak value, gaining an additional 25 keV of energy. There was no reason why more gaps could not be used in the same arrangement to produce a higher final energy. Also, since the exterior of the device was grounded, multiple sections could be combined. This experiment demonstrated how alternating voltages can produce final beam energies greater than that achieved in an electrostatic accelerator.

After World War II, high power microwave sources became available. Using a higher frequency voltage source in the Wideröe design had the advantage of reducing

the length of the drift tubes needed. The disadvantage was that there would be significant radiation losses at high frequencies because of the unshielded capacitive gaps in between the drift tubes [9]. A solution proposed by Alvarez was to excite a large cylindrical cavity containing drift tubes inside to shield the particle during half of the RF cycle. The Alvarez structure may be viewed as several short cylindrical cells coupled to each other and oscillating in phase. The currents flowing along the wall shared between two neighboring cells will cancel each other completely, rendering the walls superfluous.

Another major advancement in linear particle acceleration was the method of launching a travelling wave with a velocity equal to that of the particle [8, Sec.1.1]. The longitudinal electric field of the travelling wave would continually push the particle, transferring energy to it. A single cylindrical tube cannot accomplish this, since the phase velocities of the waveguide modes are greater than the speed of light. A periodic placement of disks with holes cut in the center for the beam are used to reduce the phase velocity to the speed of light. Such a structure may be viewed as a series of cylindrical cells, with each cell coupled to its nearest neighbors. This method of particle acceleration was eventually used at the Stanford Linear Accelerator Center.

An alternative method for accelerating a beam with coupled cylindrical cells is to form a series of independent multicell cavities. Each cavity is independent in the sense that it is powered separately with its own adjustable amplitude and phase. A standing wave is established in each cavity, with the electric field in each cell 180° out of phase with respect to both of its neighboring cells. The length of each cell is set to $\frac{\beta\lambda}{2}$ where β is the particle velocity divided by the speed of light and λ is the speed of light divided by the RF frequency. This cell length ensures that the particle is in a given cell for half of the RF period and can therefore be accelerated by the electric field in every cell. This is the method used for superconducting cavities and has the operational advantage of greater flexibility: each individual cavity may be adjusted as needed or even shut down if necessary.

One of the primary characteristics of all linacs is the ability to produce high-energy, low-emittance beams. In circular machines such as electron storage rings, the emittance of the beam is determined by the synchrotron radiation emitted in the bending magnets. The emittance of the beam in a linac is essentially determined by the source, not the machine lattice. Some other advantages of linacs [8, Sec.1.1]:

1. Strong focusing can easily be provided to confine a high-intensity beam.
2. The beam experiences a single pass, avoiding resonances which can occur when beam is fed back in a circular machine.
3. The final energy of the beam is not limited by synchrotron radiation losses since there are no bending magnets.
4. Injection and extraction are simpler.
5. A linac can operate at any duty factor, including CW.

1.1.1 Energy Recovery Linacs

Superconducting cavities allow large electron beam currents which can be used for applications such x-ray free electron lasers (FELs) and electron cooling of a heavy ion beam. The low emittance electron beam of a linear accelerator is capable of producing very bright, coherent x-rays. However, FELs only convert approximately 1% of the available beam energy to x-ray energy. For example, a 10 kW laser would require 1 MW of beam power, with 990 kW of beam power left over after lasing. Simply disposing this high-energy, high-power beam would be economically unattractive and would produce enormous amounts of radioactivity at the beam dump. Energy recovery is a method to generate a high-energy, high-current beam using only a small fraction of the available beam power.

The concept is to first start with a high-energy, low-emittance source of electrons, such as an RF or DC photo-injector. Electron bunches leave the source with speeds

near that of light. They are then further accelerated, providing the power that the application, such as lasing or cooling, will later extract. The bunches are then accelerated to high energy through a main linac consisting of several independently phased cavities. After reaching high energy, the bunches are used for the intended application. Bending magnets then recirculate the beam back to the main linac. The bunches enter the main linac 180° out of phase with the RF, so the bunches decelerate, giving their energy back to the cavity mode. When the bunches leave the main linac, they have the same relatively low energy they started with when they left the source, and can be safely dumped. The cavities in the main linac act as energy storage devices. The energy stored in the accelerating mode will decrease during the first half of an RF period when a bunch is being accelerated, but the energy will be restored during the second half of the RF cycle as a subsequent bunch is decelerated. Averaged over an RF period, the net beam loading of the cavity is zero, and power must only be supplied to compensate for the dissipative losses of the cavities. The situation is analogous to reactive elements in a lumped circuit, where the instantaneous power going into or out of the element can be large but there is no net power consumed by the lossless element.

1.2 Radio-Frequency Cavities

An RF cavity is essentially a closed metal structure which uses one of its electromagnetic modes of oscillation to accelerate beam. A standing wave is established in which the field pattern has an electric field pointing primarily in the direction that the beam travels. By driving the cavity at the mode's resonant frequency, the relatively small field of the forward travelling wave from the power supply can result in a large field in the cavity. The only power which must be externally supplied is to compensate for the dissipative losses of the metal walls of the cavity and the power transferred to the beam. The basic shape used for superconducting cavities and the salient features of

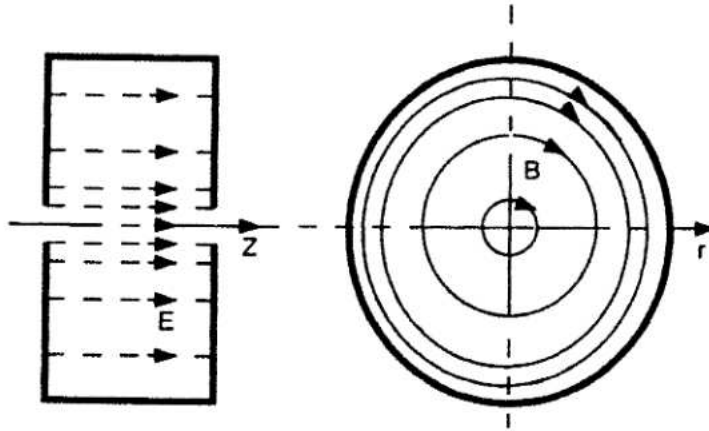


Figure 1.1: The TM010 field pattern has a large electric field along the beam axis [8, Sec.1.2].

the accelerating mode field pattern will be described in the following section.

1.2.1 The Elliptical Cavity

As the name implies, the pillbox cavity is a cylinder with the diameter larger than the radius. The lowest frequency resonant mode for such a structure is the TM010 mode. As can be seen in Figure 1.1, the electric field along the beam axis is very high. The electric field is highest along the beam axis if there is no hole to allow the beam to pass through the cavity. When an opening is made for the beam pipe, the peak electric field will occur along the surface of this opening. The peak magnetic field occurs at a radius that is approximately 73% of the cavity's outer radius. For superconducting cavities, all corners are rounded with an elliptical profile. The purpose of rounding the corner at the iris is to reduce the peak electric field and therefore reduce the chance of field emission occurring at high field. The purpose of rounding the outer equatorial edge is to avoid hard multipacting barriers and reduce the peak magnetic field on the surface of the cavity. Large surface magnetic fields are maintained by large electrical currents on the surface and therefore locally dissipate large amounts of power. If this heating occurs near a defect in the material, the increased temperature could initiate a thermal instability which destroys the superconducting state. Figure 1.2 shows the

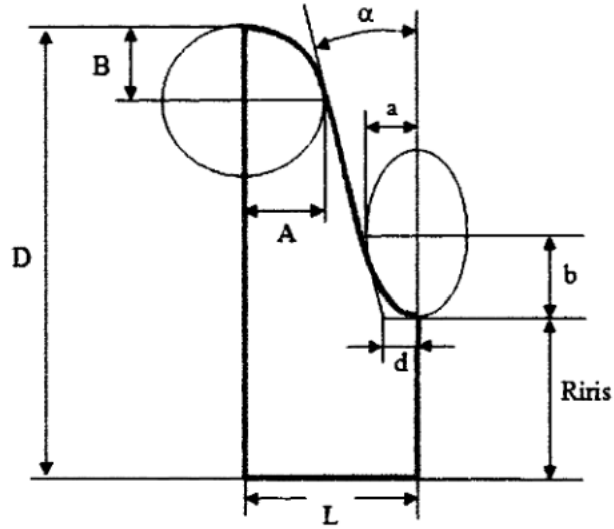


Figure 1.2: An elliptical profile is used for the equator and iris of the cell with a straight section connecting the two ellipses.

geometrical parameters which characterize the cell shape:

D = equatorial radius of the cell. It is adjusted primarily to tune the resonant frequency to the design value.

L = half-length of the cell. It is set equal to $\frac{\beta\lambda}{4}$, where β is the particle velocity divided by the velocity of light and λ is the speed of light divided by the resonant frequency.

R_{iris} = beam tube radius.

α = angle that the straight section connecting the two ellipses makes with the vertical.

d = location where the straight section would intersect the beam tube if both were continued indefinitely.

a = minor semi-axis of the iris ellipse.

A = minor semi-axis of the equator ellipse.

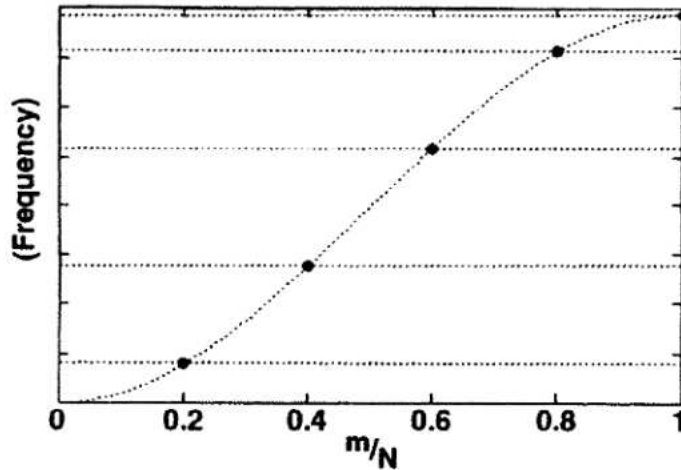


Figure 1.3: The dispersion diagram for the TM01 passband [10, p.134].

b = major semi-axis of the iris ellipse.

B = major semi-axis of the equator ellipse.

Several elliptical cells are welded together to form a single multicell cavity. The TM010 mode of a cell couples to those of its neighboring cells via the electric field. This coupling causes the TM010 mode to split into a passband of closely spaced modes equal in number to the number of cells. The dispersion diagram for the TM010 passband of a hypothetical 5-cell cavity is shown in Figure 1.3.

The width of the passband (range of frequencies of the modes in the passband) is determined by the strength of the cell-to-cell coupling, which is primarily determined by the iris radius. A longer cavity with more cells would have more modes in the same frequency range, therefore increasing the number of cells reduces the difference in frequency between the adjacent modes of the passband.

Figure 1.4 shows an example of a 5-cell cavity, illustrating the electric field lines for the accelerating mode. The accelerating mode has the highest frequency in the passband and is referred to as the π -mode since the phase advances by 180° from cell to cell. The field pattern in each cell is TM010 for the accelerating mode. The higher-order modes have their own passbands, and the field pattern in each cell is

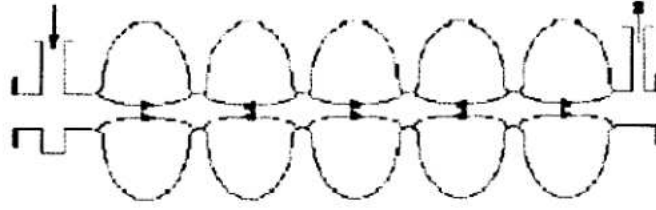


Figure 1.4: Conceptual schematic showing the alternating electric field lines of the π -mode [10, p.4].

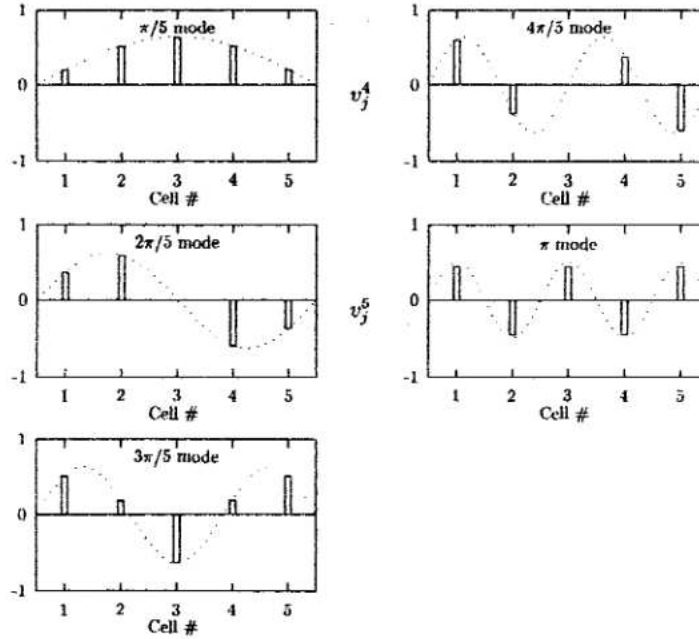


Figure 1.5: The modes within a passband are characterized by the sinusoidal variation in electric field amplitude from cell to cell [10, p.132].

that of the HOM. All passbands will contain as many modes as there are cells. For the m^{th} passband mode, the amplitude in the j^{th} cell is proportional to

$$\sin \left[m\pi \left(\frac{2j-1}{2N} \right) \right] \quad (1.1)$$

where N is the total number of cells in the cavity. This variation in cell amplitude is graphically depicted in Figure 1.5 for the case of a 5-cell cavity.

1.2.2 Superconductivity

There are several advantages to using superconducting (SC) cavities made from bulk niobium instead of normal-conducting (NC), copper cavities for particle accelerators [10, Sec.1.2]. High gradients may be achieved with both technologies, but the mechanical properties of copper and the quality of the cavity vacuum degrade if a copper cavity's temperature exceed approximately 100°C. To prevent excessive heating at high gradients, the duty factor is typically lower than 1%. Because the Q of a SC cavity is typically 10^5 times greater than a copper structure, high gradients are possible at high duty cycles and up to CW operation. The high Q of SC cavities reduces the power dissipated, in the range of 1-10 W. This power must be dissipated at cryogenic temperatures however, which is inherently inefficient due to the low Carnot efficiency of refrigeration at or below 4 K. When the Carnot efficiency is combined with the mechanical efficiency of the refrigeration system, the overall efficiency is approximately 0.3%. However, when the efficiency of the klystron used to power a NC cavity is taken into account, a SC structure would require approximately 200 times less AC wall power to operate than a NC structure at the same duty cycle. The high Q also enables larger cavity apertures to be used, which significantly reduces any interactions between the beam and the cavity HOMs. The beam will deposit less energy in the HOMs; The HOMs will degrade the beam emittance less and higher beam currents can be accelerated before HOM-induced beam instabilities arise. Larger apertures thus allow for higher average beam currents.

SC cavities bring not only improved performance but also additional challenges. To attain high Q 's, cleanliness during fabrication and processing of bulk niobium SC cavities is crucial. The power per unit area dissipated locally on the inner surface of a cavity is given by the expression

$$P = \frac{1}{2}R_s H^2, \quad (1.2)$$

where H is the local magnetic field on the surface and R_s is the surface resistance. The BCS theory of superconductivity predicts that at temperatures below half of the critical temperature, the surface resistance has the approximate form [10, Sec.3.4],

$$R_{\text{BCS}} = A\omega^2 e^{-\frac{\Delta(0)}{k_B T}}. \quad (1.3)$$

Here ω is the angular frequency of the RF, $\Delta(0)$ is the energy gap at zero temperature, k_B is Boltzmann's constant, T is the temperature, and A is a temperature and frequency independent constant whose value is determined by the properties of the material. The surface resistance measured in experiments is consistent with the BCS prediction, therefore lowering the temperature of the helium bath can dramatically reduce the surface resistance. However, the decrease in surface resistance with temperature does not continue indefinitely. Eventually the measured surface resistance reaches a constant value independent of temperature. This residual resistance (R_o) is essentially due to impurities and foreign material on the niobium surface or trapped magnetic flux. The surface resistance of a SC cavity therefore has the form

$$R_s = A\omega^2 e^{-\frac{\Delta(0)}{k_B T}} + R_o. \quad (1.4)$$

The value of R_o typically attained is in the range of 10 to 20 n Ω . For cavities operating at frequencies around 1.5 GHz, the temperature must be less than or equal to approximately 2 K for the BCS resistance to drop below this level [10, Sec.9.1]. To achieve these low limiting values of surface resistance and to ensure adequate rates of heat transfer to the helium bath, careful precautions must be taken.

The BCS resistance has a strong dependence on temperature, so it is desirable to increase the rate of heat transfer through the bulk niobium as much as possible to ensure that the temperature rise from the outer to inner surface is as small as possible. Electron-phonon scattering essentially determines the value of both the

electrical and thermal conductivities of a metal at room temperature. These conductivities are higher at cryogenic temperatures since the number of phonons is reduced [10, Sec.3.2.1]. The conductivities eventually saturate at limiting values where electron scattering with impurities dominates. Since it is relatively easy to make precise measurements of electrical conductivity, the ratio of the saturated electrical conductivity to the room-temperature electrical conductivity is used as a measure of the purity of bulk niobium. High values of this ratio, called the residual resistance ratio (RRR), are therefore desirable. High purity niobium is expensive, with the cost roughly proportional to the RRR: A RRR of 250 is typical. During the stamping of elliptical half-cells and machining of weld preps, care must be taken to avoid using steel. This prevents any iron from contaminating the surface and providing magnetic flux to be trapped during cooldown. Also, high permeability metal must be used to shield the cavity from stray magnetic fields (including the Earth's magnetic field) during cooldown. Conventional welding techniques such as tungsten-inert-gas (TIG) welding would contaminate the niobium surface, so all welds are typically done with an electron beam under high vacuum. If hydrogen concentrations are above 2 ppm by weight, then there is a risk of a lossy hydride forming on the Nb surface at temperatures between 60 K and 150 K [10, Sec.9.4]. The acid used for etching the cavity surface must be chilled below 20°C to avoid excessive hydrogen to be released on the surface. Baking at 700°C to 900°C under vacuum is necessary to ensure that hydrogen concentrations are low enough to preclude precipitation of hydrides. An alternative approach to baking, which was adopted here at MSU, mitigates the formation of the hydride by cooling down quickly (approximately 1 hour) while in the temperature range of 60 K to 150 K.

1.2.3 Issues Driving Cavity Design

Superconducting cavities are an ideal choice when large beam currents and high duty cycles are desired. These characteristics combined with the efficient use of beam power

in an ERL have lead to a number of projects striving for 100's of mA of electron beam current for use in a high power FEL or for electron cooling. The primary challenges for the cavity at these high beam currents are to reduce the amount of beam-induced HOM power as much as possible and to effectively damp the dipole HOMs that are primarily responsible for the multipass beam breakup (BBU) instabilities that ultimately limit the maximum available beam current.

If a particle enters a cavity on the central axis when a dipole HOM has been excited, then the particle will leave with a deflection in the horizontal or vertical direction. The optics of the recirculation line will cause the transverse momentum imparted to the particle by the HOM to result in the particle entering the cavity with a transverse displacement when it returns for deceleration. The transverse offset can cause the particle to further excite the HOM and this process can continue until the particle collides with the cavity wall [6]. The threshold current at which a multipass BBU occurs is predicted to the correct order of magnitude by the expression [11]

$$I_{\text{th}} = \frac{-2pc}{e \left(\frac{R}{Q}\right) QkM_{12}}. \quad (1.5)$$

Here p is the momentum of the particle, c is the speed of light, e is the charge of the electron, $\frac{R}{Q}$ is the shunt impedance of the HOM, Q is the quality factor of the HOM, $k = \frac{\omega}{c}$ is the wavenumber of the HOM, and M_{12} is the transfer matrix element relating the transverse momentum at the cavity exit to the transverse displacement of the particle at the entrance of the same cavity during the next pass. The HOM of concern is the one which corresponds to the lowest threshold current. The beam-induced power dissipated by a longitudinal HOM is given by

$$P = \frac{\omega I |q|}{4} \left(\frac{R}{Q}\right), \quad (1.6)$$

where ω is the angular frequency of the HOM, q is the bunch charge, I is the average

beam current, and $\frac{R}{Q}$ is the shunt impedance of the HOM. The goal is then to minimize both the $\frac{R}{Q}$ and loaded Q values for all HOMs which interact with the beam. In contrast, strong interactions between the cavity accelerating mode and the beam are desirable for efficient acceleration, so the general aim for this case is to maximize both $\frac{R}{Q}$ and Q .

1.2.4 Outline

This dissertation will present the design of three superconducting cavities intended for acceleration of beams with high average current. Elliptical cavities with two cells and six cells have been designed for use in an ERL. The two-cell cavity is designed for use as an injector cavity, operating without energy recovery. The six-cell cavity is suitable for acceleration in the main linac. The third cavity shape is a single cell suitable for use in an electron storage ring. All three cavities have large apertures, which reduce the HOM heat load and increase the threshold currents for beam instabilities. Chapter 2 describes the solution for general cavity fields and the key figures of merit used to describe these field patterns. The figures of merit allow one to compare different cavity shapes and judge which shape is better for an intended application. The figures of merit are therefore important for understanding the design goals of the three different cavities. Chapter 3 describes the design criteria for the shape of the six-cell cavity and the method used to meet these criteria. Here the basic approach to avoiding HOM-induced beam instabilities is described and will constitute one of the primary design criteria. Chapter 4 describes the design and shape of the two-cell cavity. Two copies of the two-cell cavity shape were prototyped and tested. The details of this fabrication process and the results of the tests are presented. Chapter 6 describes the basic concept of using a HOM in a single cell cavity as the accelerating mode. The purpose of using the HOM is that it allows the aperture of the cavity to increase significantly without significantly increasing the heat dissipated in the accelerating mode. The increased aperture has the advantage of diminishing interactions between

the undesirable HOMs and the beam and therefore enabling larger beam currents to be used.

